Journal of GeoEngineering, Vol. 18, No. 3, pp. 159-173, September 2023
http://dx.doi.org/10.6310/jog.202309_18(3).6

EFFECTS OF EARTHQUAKE-INDUCED SEDIMENT EJECTA ON DYNAMIC STABILITY OF LEVEE CONSTRUCTED OVER LIQUEFIABLE GROUND

Aparna Kanth [1] and Ritesh Kumar [2*]

ABSTRACT

Sediment ejecta is a mechanism that significantly contributes to the severity of liquefaction-induced ground failures. Consequently, it is essential to quantify the hydraulic demand and qualitatively estimate the sediment ejecta for assessing the ground failure severity. However, the methodology for this quantification has not been thoroughly studied. Evaluation of sediment ejecta provides an accurate estimate for adopting cost-effective and reliable measures for soil strengthening. The problem of sediment ejecta could be more severe if it occurs on the constructed ground surrounded by a residential area, as it would affect the build area and human life. Therefore, for the present study, a levee constructed over the level ground of dimensions 20 m × 10 m is analysed under plain strain conditions using the finite element method. For a better understanding of the behaviour, the effective stress analysis (ESA) is conducted on two models: soil Model 1 without a levee and soil Model 2 with a levee. In both instances, the hydraulic demand (AFP, Artesian Flow Potential), ground failure severity (EPI, Ejecta Potential Index) and the flow path of pore fluid are estimated. Observations indicate the occurrence of sediment ejecta in both the cases leading to extreme ground failure conditions. The hydraulic demand with levee is 5.49 m^3 producing upto 680 $m^3 \cdot s$ of EPI, which is significant to cause huge sediment ejecta and create extreme ground failure condition. It drags the attention towards the need to study the sediment ejecta manifestation and its effects on levee. Additionally, the flow path of pore fluid is also studied, indicating a diversion of pore-water flow towards the region of high permeability due to the levee's construction. The findings of Finite Element (FE) based effective stress analysis corroborate that the construction of a levee on the liquefiable ground causes sediment ejecta during an earthquake. Major contributing factors include soil densification, ground non-uniformity due to differential permeability between soil layers, and additional overburden from levee. Because of these combined factors, the ejected sediment creates a discontinuity within the soil model. It is evident from the flow path of pore fluid in Model 2, which highlights the ground's discontinuity, affecting the levee's dynamic stability. Therefore, methods need to be proposed to strengthen the soil and increase its stiffness, providing more stability to levee.

Key words: sediment ejecta, hydraulic demand, levee, liquefaction, excess pore pressure, artesian water pressure, flow path.

1. INTRODUCTION

The Canterbury Earthquake Sequence occurred in 2010-2011 reported several cases where buildings experienced huge differential settlements. These failures to were caused due to a post liquefaction phenomenon also referred to as sediment ejecta. The process of sediment ejecta starts from the dissipation of excess pore pressure (u_e), which triggers high-gradient upward seepage that may produce artesian flow. A typical soil profile is presented, showing its condition before the earthquake in Fig. 1(a) and during the earthquake in Fig. 1(b). The stable layers of soil at rest are shown in Fig. 1(a), where pavement is underlain by the consecutive crust layer, sediment layer and loosely packed granular layer. On the contrary, Fig. 1(b) shows the traces of sand boils emerging onto the ground surface through the cracks. Higher u_e provides a hydraulic gradient that commences groundwater seepage from higher to lower level of total hydraulic head. With a sufficient hydraulic gradient (i), upward seepage can uplift the soil particles, trigger heaving (directing to quick-sand condition) or piping (referred to cracking of the top crust layer), and produce ejecta. During the advection process, liquefied material is transported vertically or laterally through seepage, generating voids at specific locations where the ground may sag dramatically. The greater the volume of sediment delivered to the ground, the larger the cavity, leading to more severe ground failure. Lowe (1975), Seed (1979), NAS (1985), and NAS (2016) contribute significantly to our understanding of the mechanism of sediment ejecta.

Early studies by Housner (1958) and Ambraseys and Sarma (1969) have shown that sediment ejecta is produced due to the dissipation of excess pore pressure generated during earthquake. The authors noted that sediment ejecta occurs several minutes after the earthquake has ceased shaking, suggesting it to be a post-shaking event. The delay is the time required for upward seepage-induced piping to occur inside the upper crust layer before the release of liquefied material onto the earth's surface. The ejection can reach a height between 305 and 610 mm above the ground and produce gigantic sediment ejecta, a volcano measuringup to 6 m in diameter.

Manuscript received February 13, 2023; revised July 3, 2023; accepted July 6, 2023.
[1] Research Scholar, Department of Earthquake Engineering, Indian Institute Technology Roorkee, Roorkee, India.
[2*] Assistant Professor (corresponding author), Department of Earthquake Engineering, Indian Institute Technology Roorkee, Roorkee, India (e-mail: ritesh.kumar@eq.iitr.ac.in).

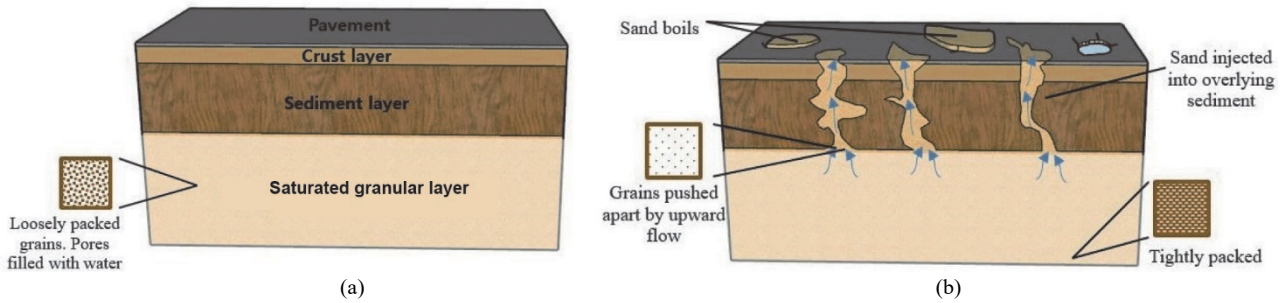

Fig. 1 A typical soil profile showing sediment ejecta manifestation: (a) Before earthquake; (b) During and after the earthquake

Housner (1958) reported the flow of sediment ejecta a few minutes after the 1934 Bihar, India earthquake got initiated. Ambraseys and Sarma (1969) reported 1964 Niigata earthquake caused the ground to crack 2 to 3 minutes after its beginning. The water flow began, ascended to a height of 1.5 m, and continued for around 20 minutes. It contained the fluidised sediment, which was found to eject from 4.5-6 m depth within the ground. The Loma Prieta earthquake of 1989 generated considerable sediment ejecta in San Francisco's Marina District (Bardet and Kapuskar 1993). In Marina District, the largest sand boils were measured that stretched around 29 m^2 and had sediment heights between 10 to 20 cm. Examples of a well-documented sand boil include the 1995 Kobe earthquake (*e.g.,* Soga 1998 and Cubrinovski *et al.* 2019). Strong ground motion at the Port Island station is another valuable case history site to examine the liquefaction by a large number of scholars thoroughly. Sediment ejecta covered the surrounding strong motion station, where ground subsidence of 300-400 mm was reported, and the height of sediment ejecta was observed to be 150-200 mm. The Canterbury and Tohoku earthquake in 2011 generated voluminous documentation of sediment ejecta. There are several studies such as those carried out by Tobita (2019) and Tsai *et al.* (2022), where settlements followed by sand boils are observed and studied. Takano *et al.* (2016) have also discussed sand boiling and localized settlement based on the centrifuge modelling to simulate liquefaction on multi-layered sandy ground; Kawai *et al.* (2017) have conducted the shear box tests and related the critical strains with the amount of soil erupted during sand boils. Substantial amounts of ejecta were recorded on level terrain in the city of Kamisu. Sediment ejecta covered nearly the entire city (1,000-10,000 m^2) and triggered severe ground failures (Ashford *et al.* 2011). As much as 2 m of the ground sinking was reported. Similar behaviours were reported following the February 2011 earthquake in Christchurch, New Zealand by Hutabarat and Bray (2019), where post-shock upward seepage induced heaving in regions of level ground (Fig. 2(a)). At specific locations, upward seepage can raise groundwater levels to the ground surface. In many instances, the ground became much softer, resulting in buoyancy or quicksand, which implies loss of all bearing capability. When the deposits of sand restore their strength, extracting a light object, such as a sunk automobile, from the soil becomes difficult (Fig. 2(b)).

For estimating the severity of ejecta manifestation, the liquefaction severity number (LSN) and liquefaction potential index (LPI) are extensively used indices. As documented by Maurer *et al.* (2014); Van Ballegooy *et al.* (2015) and Cubrinovski *et al.* (2019), however, these indexes frequently either underestimate or overestimate the results. However, the simplified liquefaction ground-failure indices are useful for assessing the probability of ground collapse, but their inability to produce reliable findings necessitated the development of alternative approaches, as described by Hutabarat and Bray (2021). The authors presented the reliable indices artesian flow potential (AFP) and potential ejecta index (EPI), which account for the hydraulic process behind sediment ejecta.

Closed-form solutions were produced by Housner (1958) and Ambraseys and Sarma (1969) to compute pore pressure distribution within soil deposits. These solutions evaluate the artesian pressure required to push the muddy water out of the ground surface. According to these researchers, estimating the u_e induced by earthquake is the crucial step in quantifying ejecta potential. Soil is a three-phase system consisting of soil particles, air voids, and water-filled voids. For saturated (2-phase system) soils, behaviour is heavily impacted by the solid-fluid interaction. Biot (1941) initially developed the equation that governs the solid-fluid interaction for the consolidation problem (theory of porous media) and then extended it for dynamic situations (*e.g.,* Biot 1956; Biot 1962a; Biot 1962b). Zienkiewicz and Shiomi (1984) generalised Biot's equations and provided a finite element method-based solution methodology. The governing equations are separated into three general linked formulations based on the unsolved unknown dependent variables: (1) u-p, (2) u-U, and (3) u-p-U, where u represent solid displacement, p represents pore fluid pressure, and U represents pore fluid displacement. ESA is described as a numerical approach for solving coupled equations in which the unknown variables for each formulation are computed simultaneously at each time step.

(a) Aerial shot shows damage due to liquefaction and induced sediment ejecta (image from www.issmge.org).

(b) Sunk vehicles due to widespread sediment ejecta (image from www.sciencelearn.org).

Fig. 2 Impact of the Christchurch 2011 earthquake, New Zealand: (a) Aerial shot shows damage due to liquefaction and induced sediment ejecta; (b) Sunk vehicles due to widespread sediment ejecta

Hutabarat and Bray (2021) reported that the severity of liquefaction-induced ejecta manifestation for the 2010-2011 Canterbury earthquakes was either overestimated or underestimated using liquefaction vulnerability indices, such as the Liquefaction Potential Index (LPI) or Liquefaction Severity Number (LSN). These misestimations are overcome by introducing two new indices, the Artesian Flow Potential (AFP) and Ejecta Potential Index (EPI). These concepts are formulated to capture this post-shaking hydraulic mechanism. The excess hydraulic head profile with depth that develops during and after earthquake shaking determines the potential of upward seepage-induced piping that produces sediment ejecta.

2. PROBLEM STATEMENT

The Roorkee region of Uttarakhand, located in the heart of India (as shown in Fig. 4), is considered for the present study. The site lies in seismic zone IV (as per IS 1893 (Part 1): 2016) and is prone to liquefaction, hence it is essential to study its dynamic effects on existing and proposed structures. A levee structure is constructed in the Roorkee region, surrounded by the Solani river and a residential area on its left. Solani sand is more likely to liquefy due to its characteristic properties defined by in-situ and element testing. The properties of Solani sand collected during Standard Penetration Tests (SPT) are determined by basic laboratory tests conducted by Kirar and Maheshwari (2018) as listed in Table 1. As shown in Fig. 3, the grain size distribution (GSD) curve of the soil used to prepare test samples is determined by passing it through a 1.18 mm sieve. The examined soil sample is characterized as poorly graded sand (SP) based on the particle size distribution.

Table 1 Index properties of Solani sand (from Kirar and Maheshwari (2018))

Property	Notations/Unit	Values
Soil type		Solani sand
Classification	SP	Poorly graded sand
Specific gravity	G_s	2.68
Uniformity coefficient	C_u	1.96
Coefficient of curvature	C_c	1.15
Grain size (mm)	D_{10}	0.12
	D_{30}	0.18
	D_{50}	0.210
	D_{60}	0.235
Minimum void ratio	e_{min}	0.54
Maximum void ratio	e_{max}	0.85

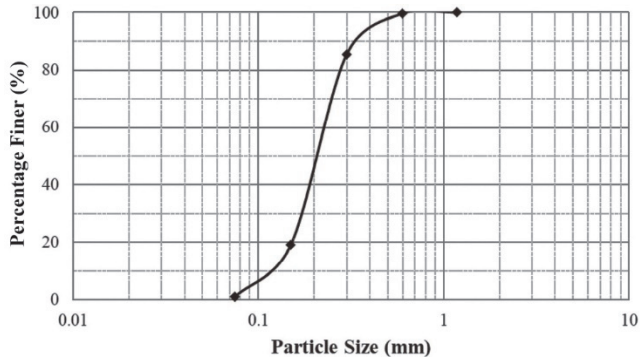

Fig. 3 Grain size distribution for Solani sand: uniformly distributed grain size classified soil as poorly graded sand (SP)

Moreover, if the soil liquefies, there is a possibility of sediment ejecta, which may affect the livelihood of the adjacent residential area. It was the motivation to study the liquefaction behaviour of Solani sand, safeguard residents' lives, and suggest cost-effective measures to strengthen the soil. Sediment ejecta manifestation during liquefaction would not only allow for the preparedness of expected damage due to failure of the existing structures, such as the levee. However, it would also help to propose measures to strengthen the soil for upcoming projects. For instance, at a 6 km stretch from this levee, there is an upcoming project for a buried sewage pipeline to be constructed over the Solani river. This project is proposed in the south-eastern region of Uttarakhand, extending to several km from Saharanpur. The pipeline is expected to cross the Solani river in Sundhari village. A levee constructed over the soil model (20 m wide and 10 m deep) is analyzed under plain strain conditions. It is necessary to first examine the dynamic behaviour of level ground to comprehend the dynamic behaviour of levee on level ground. Thus, the effective stress analysis (ESA) is carried out for two cases: Model 1 without a levee and Model 2 with a levee. In both cases, post-liquefaction dynamic behaviour is studied by estimating the hydraulic demand and corresponding sediment ejecta. For a better understanding, the flow path of pore fluid is also studied.

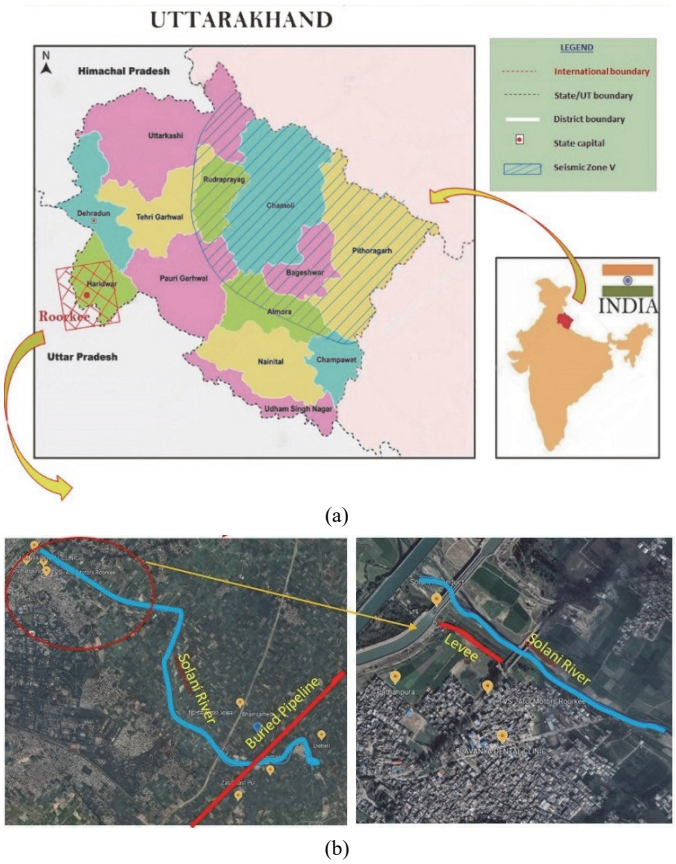

Fig. 4 Location map of the study area; (a) Uttarakhand lies in northern India, with Roorkee as a small city in Uttarakhand. The hatched area in the province map corresponds to Zone V of the Earthquake Zoning Map of India. In contrast, the unhatched area pertains to Zone IV (as per IS 1893 (Part1): 2016), (b) Locationof levee constructed over Solani river considered for analysis in Roorkee

Before the assessment of sediment ejecta, understanding its origin is essential. When an earthquake occurs, there is a development of excess pore pressures (u_e) (EPP), which gets simultaneously dissipated. This dissipation is minimal at the initial stages but gets noticeably large soon after the point of liquefaction. The dissipation of EPP can cause high-gradient upward seepage, which can cause cracks in the upper soil layers. Upon adequate artesian water pressure development, the artesian flow may be generated via upward seepage flow. Simultaneously, the sediment ejected is observed at the ground surface. It causes the ground to settle, and the magnitude of this ground subsidence is proportional to the quantity of sediment ejected.

The model geometry is built to carry out the non-linear effective stress analysis for the current investigation, and AFP is computed to measure the hydraulic demand to cause sediment ejected. This phenomenon is found effective up to 10 m of depth from the ground surface and usually occurs a few minutes after an earthquake occurs. Once the AFP is evaluated for the level ground, the analysis is further extended to assess the effect on the levee resting over the level ground. Based on the flow conditions achieved, soil conditions can be strengthened by providing a discontinuity or gravel channel to increase the stiffness of the soil.

3. ANALYSIS SCHEME

A pre-defined workflow as shown in Fig. 5 is followed for the sediment ejecta manifestation. Initially, the Roorkee region is chosen for the present study as a site prone to liquefaction. Further,

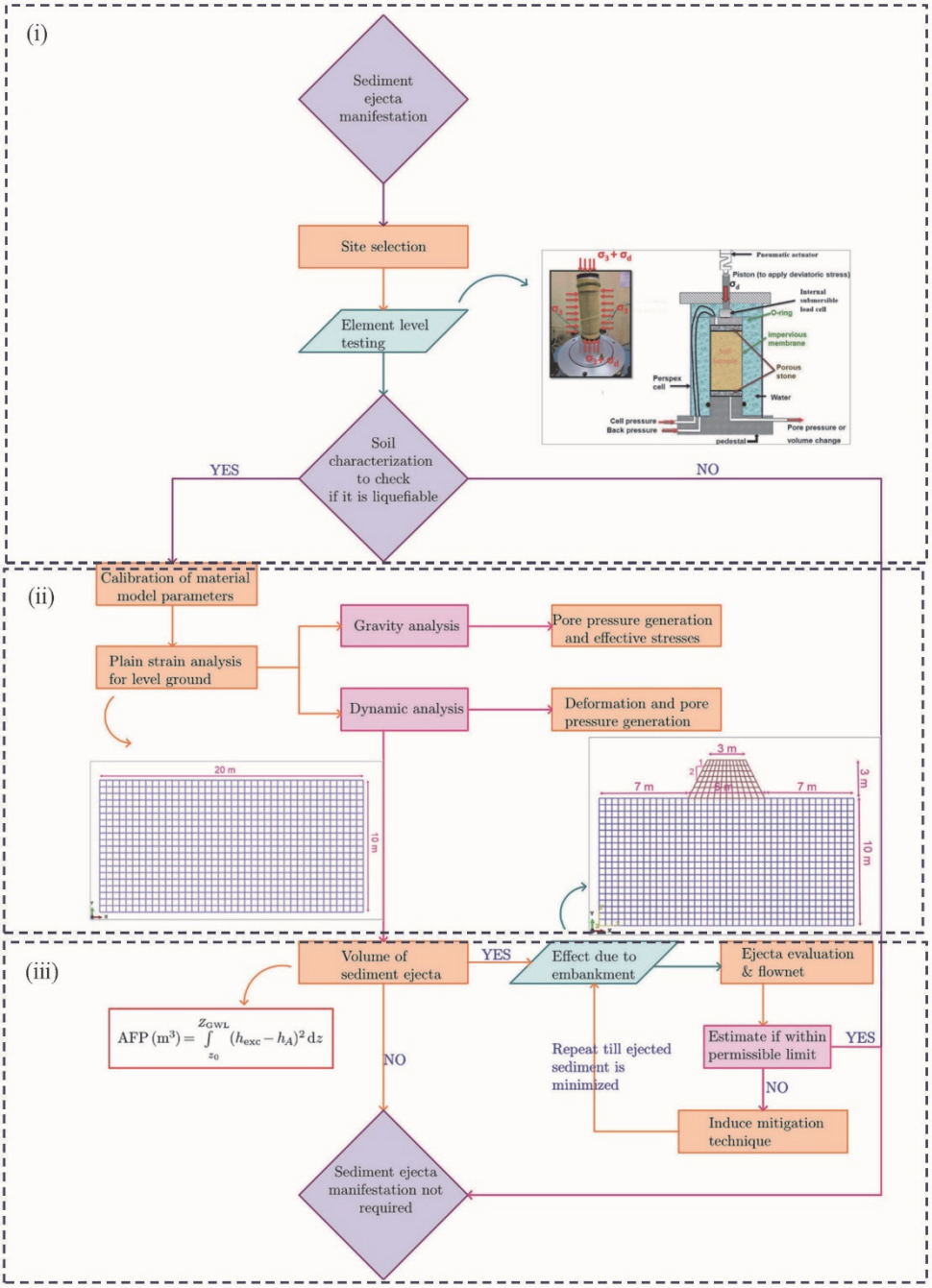

Fig. 5 Flow of work for sediment ejecta manifestation: comprises of three parts: (i) Experimental soil characterization; (ii) FE-based effective stress analysis; and (iii) sediment ejecta estimation and study of flow-path of fluid

element-level tests are carried out on cyclic triaxial for the quantification of soil liquefaction susceptibility. In the case of non-liquefiable soils, ejecta manifestation is not required. However, in the case of liquefiable soils, there could be a possibility of sediment ejecta which may affect the build environment. Therefore, its manifestation is required and effective stress analysis is carried out on such liquefiable soils. Initially, parameters for the selected constitutive soil model are calibrated with element-level testing. Then the calibrated parameters are used for gravity and dynamic analysis of considered Model 1 (without levee). Utilizing the generated excess pore pressures and respective excess head, artesian flow potential (AFP) is determined using Eq. (3) as discussed in proceeding Section 3.4. AFP estimates the hydraulic demand to cause sediment ejecta post-liquefaction. If estimations show that the hydraulic demand is not sufficient enough for sediment ejecta, further evaluations may not be required. Elsewise, AFP is further determined in the case of Model 2 (with levee). The concept of AFP was created to assess the hydraulic demand (or necessary artesian pressure, *i.e.,* post-shaking water flow) and initiates the artesian flows that eject the liquefied sediment. The AFP index identifies distinct time points when $h_{exc} > h_A$. However, according to the field research, it is suggested that more sediment is ejected through the ground surface if the artesian flow persists for a longer duration. Thus, duration is an important key for consideration in assessing the potential of artesian flow and ejecta. The time history of AFP is integrated over time to capture the important influence of duration to define another important evaluation parameter Ejecta Potential Index (EPI), which is also discussed in proceeding Section 3.4. The flow path of pore fluid is also studied for both cases. If the value lies within permissible limits (qualitatively discussed in Section 4), there is no further need for manifestation. In the case of impermissible values, mitigation techniques are proposed, and the analysis is again performed for evaluation. This process is repeated till the soil gains sufficient strength to have the permissible sediment ejecta.

3.1 Model Description

A soil model of dimension 20 m in width to 10 m in height, as shown in Fig. 6(a), is prepared as a Model 1 (without levee) for analysis. The bottom nodes are fixed in all degrees of freedom to measure the relative settlement of overlying soil. Equal DOF is assigned to the left and right nodes to enforce the two-side boundary moving laterally and synchronizing. All nodes above 2 m depth are considered dry nodes for the consideration of the water table at 2 m. The element type used creates 861 nodes and 800 elements.

The Model 2 (with levee) is prepared such that the vertical axis of symmetry remains the same as Model 1, as shown in Fig. 6(b). The element type used creates 965 nodes and 884 elements. All nodes within the levee are considered dry. Equal DOF is assigned to the nodes of the leftmost boundary of the model and the respective nodes of the rightmost boundary of the model.

PM4SAND is a soil constitutive model designed to study the liquefaction behaviour of soil under plane strain condition. It is used in the present study, to model the behaviour of Solani sand for both the cases (Model 1 and Model 2). PM4SAND is a 2D constitutive model proposed by Boulanger and Ziotopoulou (2015). It follows the plasticity framework proposed by Manzari and Dafalias (1997), and the effect of soil composition on the shear-strain accumulation proposed by Dafalias

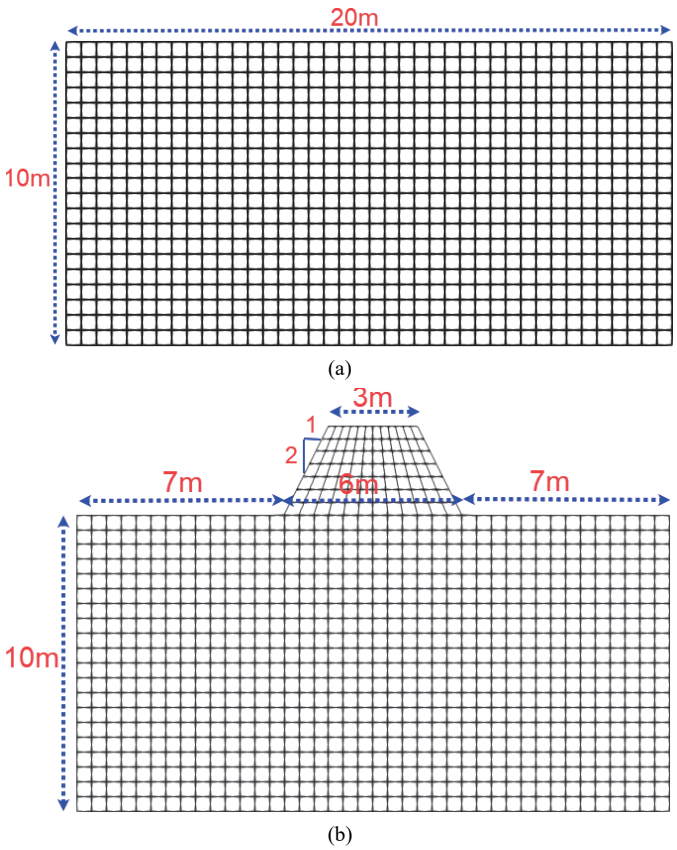

Fig. 6 Meshed model with and without levee (a) Model 1 without levee; (b) Model 2 with levee

and Manzari (2004) is also accounted for. PM4SAND constitutive model for soil implemented by Chen and Arduino (2020) in OpenSees is based on bounding surface plasticity and critical state concepts. The concept of critical state soil mechanics (CSSM) given by Been and Jefferies (1985) forms the basis for deriving PM4SAND and follows the empirical critical state line of Bolton (1986). The input parameters utilised in PM4SAND are categorised into primary and secondary parameters as listed in Table 2 (paramter calibration as discussed in Section 3.2).

Both the models (Model 1 and Model 2) are uniformly meshed considering SSPQuadUP (8-noded) element. The maximum length of the soil element (L_e) is calculated by the maximum frequency (f_{max}) of excitation that needs to be propagated through the soil. The length of the element is calculated based on the fundamental frequency using below Eq. (1):

$$L_e \le \frac{\lambda_{min}}{a} = \frac{v_s}{a \times f_{max}} \tag{1}$$

where λ_{min} is the minimum wave length of the shear wave, v_s is the shear wave velocity of soil, and a is the factor varying from 5 to 8. To capture the shortest wavelength, a factor equal to 8 is considered. The mesh size is considered after the mesh size sensitivity analysis. For sensitivity analysis, mesh size is varied from 0.25 to 1.5, and 0.5 seem to be the optimum mesh size, where the minimal deviation of results is observed. Therefore, the size of the mesh is taken as 0.5 m, which is uniform throughout the model.

Each node of the SSPQuadUP element has three degrees of freedom (DOF), two for displacement in horizontal (u_x) and

vertical (u_y) directions and a third DOF assigned for pore-pressure. The SSPquadUP element is an extension of the SSPquad Element for use in dynamic plane strain analysis of fluid saturated porous media. A mixed displacement-pressure (u-p) formulation is used, based upon the work of Biot as extended by Zienkiewicz and Shiomi (1984). Unlike QuadUP element, a stabilizing parameter α is employed to permit the use of equal-order interpolation for the SSPquadUP element. The physical stabilization allows for reduced integration and results in an element which is free from volumetric and shear locking. The elimination of shear locking results in greater coarse mesh accuracy and also analysis times are generally faster than corresponding full integration elements. The parameter α used for the mixed displacement-pressure fields in SSPquadUP element can be computed using Eq. (2).

$$\alpha = \frac{0.25 \times h^2}{\rho_s \times c^2} \tag{2}$$

where h is the element size, c is the speed of elastic wave propagation in the solid phase, and ρ_s is the mass density of the solid phase.

3.2 Parameter Calibration

The material model's parameters must be calibrated to conduct the finite element analysis, which is conducted based on strain-controlled cyclic triaxial tests. In this paper, the Effective Stress Analysis (ESA) is performed using the PM4SAND model to simulate the sand-like material and its contractive dilatation response. The primary and secondary parameters of the model influence the number of cycles required to reach liquefaction (N_{c-liq}), generation of pore pressure, the shape of the hysteretic loop, stress path and rate of shear strain accumulation. The parameters that needs to be calibrated among all primary and secondary parameters of PM4SAND are G_o and h_{po}.

As described by geotechnical test standards of ASTM, the triaxial test typically consists of four main stages: specimen and system preparation, saturation, consolidation, and shearing. Selig and Ladd (1978) presented a procedure for preparing a reconstituted sand specimen for cyclic triaxial testing. After preparing a sample of desired relative density (40%) using a mould of known diameter (D = 50 mm) and length (L = 100 mm), such that L/D = 2, the triaxial cell is filled with de-aerated water and confined cell pressure (100 kPa) was applied. The specimen is saturated before being consolidated by flushing de-aerated water through the sample under back pressure. During back pressuring, a constant low value of effective stress (approximately 12 kPa) is maintained. This low value of confining stress miminimises recorded volume changes during saturation; however, if the specimen tends to swell, a higher value should be selected. Saturation was assumed when the B-factor (ratio of change in pore pressure Δu to change in cell pressure $\Delta\sigma_c$) was ≥ 95%. The specimen was then consolidated to the required effective stress σ'_{3c}. Changes in volume and axial height were recorded during consolidation. Specimen were cyclically loaded without drainage. MTS (Material Testing and Simulation) system applied a sinusoidal varying load at a frequency of 1 Hz. The specimen was therefore subjected to a cyclically loaded under strain- controlled condition. The sinusoidal fluctuating axial deviatoric stress $\pm\sigma_d$ varied between the peak compression and peak tension values. During cyclic loading, the cell pressure was kept constant, and the changes in axial load, axial deformation and pore pressure were recorded. The general experimental set-up with specimen stress state is shown in Fig. 7.

For the calibration of PM4SAND parameters, a numerical program is developed in OPENSEES to simulate experimental results. A single column of soil is subjected to the strain-controlled sinusoidal amplitude of 0.67 mm at a frequency of 1 Hz. After 40 repetitive loading cycles, soil behaviour is studied in terms of developed stresses, strains and pore pressures.

Results for parameter calibration for 100 kPa confining pressure and 1% shear strain are as shown in Fig. 8. Experimental findings are shown in Figs. 8(a), 8(c) and 8(e) and numerical evaluations are shown in Figs. 8(b), 8(d) and 8(f). The stress-strain curves both for the sample specimen in lab and for the numerical model undergoes shear strength of at most 18 kPa. The shear strength gets mobilised within the initially prescribed strain limit of ± 1% under the strain-controlled loading. The stress-strain curves for the sample exhibits the trace of stiffness degradation of soil during the cycles of shaking. Experiments have shown that soil liquefies at six cycles, where strain accumulation occurs. The similar observations are evident from numerically obtained stress-strain curves, where stress accumulation occurs at approximately five cycles.

The stress-path shows a gradual increase in maximum shear stresses with increasing vertical effective stresses, during loading and unloading. In experimental stress-path, there is the axis of symmetry between loading and unloading stresses, which is clearly visible in numerically obtained stress-path. This is because of the seating load and initial test conditions which gets disturbed during the process of making sample saturated and consolidated in laboratory.

The excess pore-pressure generation during experimental testing is gradual in initial six cycles of loading, which become constant for further cycles. On the contrary, excess pore-pressure in numerical model in sudden for initial 5 s and becomes constant beyond that.

Thus the failure cycle or the cycle at which soil is considered to liquefy or fail is same as obtained from both experiment and numerical modelling. The analysis is repeated for other values of shear strains (0.3%, 0.5%, and 1.5%) and best fitted curve is obtained ensuring maximum value of coefficient of determination (R^2). The values of parameters, where both experimental and numerical findings are found in good agreement are adopted as the calibrated values. These calibrated parameters as listed in Table 2 are used to model soil behaviour of Solani sand in numerical modelling.

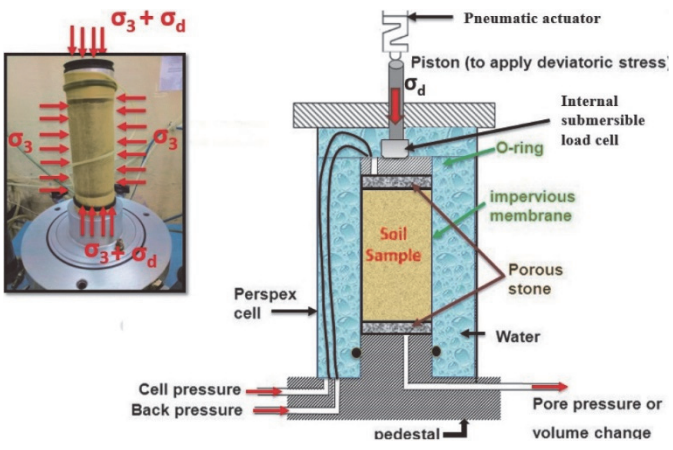

Fig. 7 Set-up for cyclic triaxial test

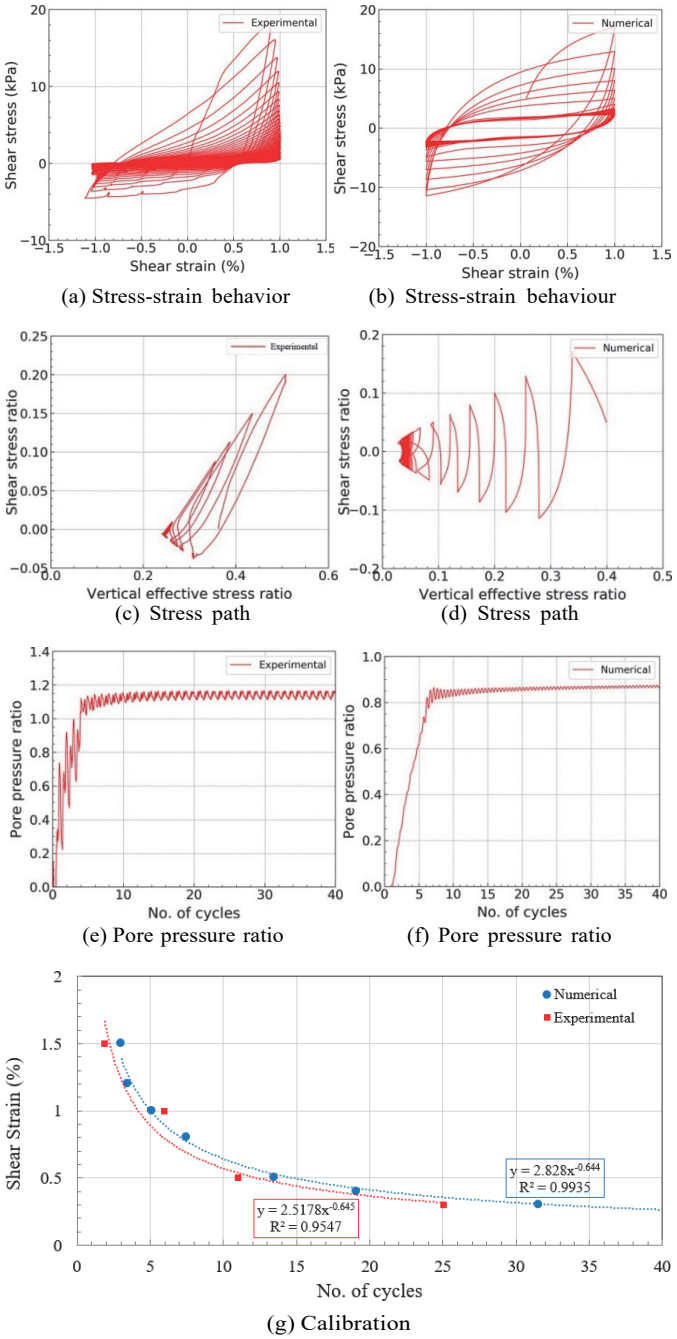

Fig. 8 Results from element-level triaxial testing for parameter calibration. (a), (c), and (e) from experiments. (b), (d), and (f) from numerical modeling

3.3 Earthquake Time History

To analyse the post liquefaction seismic response of soil; Kobe earthquake time history is applied. In past studies, damage to several levee structures is reported (Matsuo 1996; Takada *et al.* 1996; Harder *et al.* 2011; Oka *et al.* 2012 and Sasaki *et al.* 2012) during Kobe earthquake. Towhata (2014) has also presented the damaged shape of the Yodo River levee in Osaka City after the 1995 Kobe earthquake. The characteristics of Kobe earthquake such as arias intensity, frequency, magnitude, time duration, etc. are in found in compliance with the seismic characteristics of the region under consideration. The adopted earthquake motion is sufficient to liquefy soil of desired properties and induce sediment ejecta. The failure of levees and embankments constructed over the liquefied soil could thereafter be analyzed. The earthquake has a PGA of 0.34g, as shown in Fig. 9(a). The acceleration-time history is pre-dominant up to 10 s and reduces beyond that. As shown in Fig. 9(b), the derived displacement-time history gradually increases to attain its maximum amplitude of 0.09 mm at 11 s. Figure 9(c) shows arias intensity that measures the strength of ground motion and depicts that the maximum strength of motion lies between 3 to 15 s. To manually input horizontal ground motion at base of the model, it is necessary to first convert the acceleration record into its corresponding displacement time-history record, which is done in Seismosignal. Acceleration is the second derivative of displacement. And, large displacement accumulation occurs at the end of the seismic event due to erroneous indefinite integration of the acceleration time history. Therefore, while

Table 2 Calibrated primary and other secondary parameters for PM4SAND

Parameters	Symbols	Values
Primary parameters		
Shear modulus coefficient	G_o	260
Contraction rate parameter	h_{po}	6
Atmospheric pressure (kPa)	P_{atm}	101.3
Secondary parameters		
Adjusts the ratio of plastic modulus to elastic modulus	h_o	−1
Maximum void ratio	e_{max}	0.85
Minimum void ratio	e_{min}	0.54
Specific gravity	G_s	2.64
Bounding surface parameter	n_b	0.5
Dilatancy surface parameter	n_d	0.1
Dilatancy parameter	A_{do}	−1
Fabric-dilatancy tensor parameter	z_{max}	−1
Fabric-dilatancy tensor parameter	c_z	250
Adjusts the rate of strain accumulation	c_e	−1
Critical state effective friction angle (°)	ϕ_c	33
Coefficient of earth pressure at rest	k_o	0.5
Poisson's ratio	v	0.33
Adjusts degradation of elastic modulus	c_{gd}	2
Controls the rotated dilatancy surface	c_{dr}	−1
Controls the effect of sustained static shear stresses	c_{kaf}	−1
Critical state line parameter	Q	10
Critical state line parameters	R	1.5
Yield surface constant	M	0.01
Controls the minimum value the reduction factor	$Fsed_{min}$	−1
Mean effective stress (kPa)	p_{sedo}	−1
Bulk modulus of the pore fluid (kPa)	f_{bulk}	2.2×10^6
Constant body forces in x-direction	b_1	0
Constant body forces in y-direction	b_2	9.81
Spatial pressure	α	1×10^{-8}

Note: "−1" indicates the default values (Boulanger and Ziotopoulou 2015).

analyzing the model in OpenSEES, authors have preferred using displacement time-history over acceleration time-history for better analysis of the model in the finite element formulations. However, the results of the two approaches, *i.e.,* using acceleration time-history or displacement time-history will be almost the same, provided the necessary baseline correction is applied to acceleration time-history. For the understanding of soil behaviour with more clarity, output is recorded at five distinct time steps namely, $t_1 = 4.7$ s, $t_2 = 11.4$ s, $t_1 = 13.9$ s, $t_1 = 19.6$ s and $t_1 = 36.5$ s.

Using the Kobe earthquake time history, the model is subjected to horizontal input motion. Deformations and pressures are recorded at all the nodes and stresses (σ_{xx}, σ_{yy}, σ_{xy}) and strains (ε_{xx}, ε_{yy}, γ_{xy}) are recorded at the centre of each element.

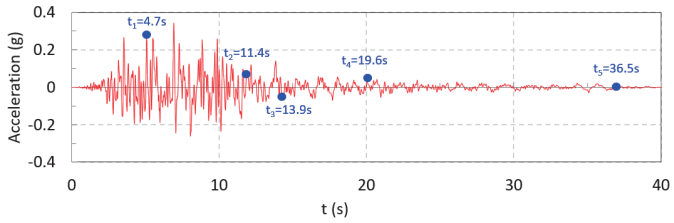

(a) North-south horizontal acceleration record

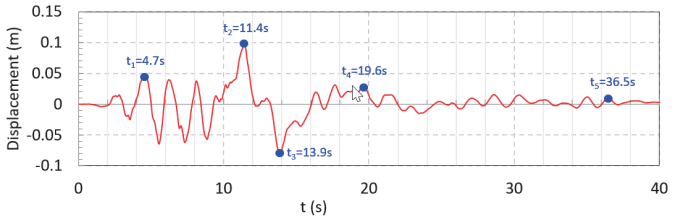

(b) Corresponding displacement-time history record

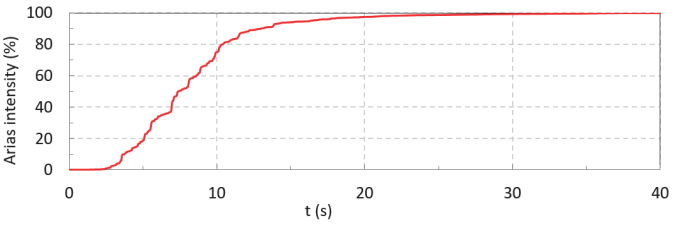

(c) Corresponding arias intensity

Fig. 9 Details of seismic waves from the 1995 M7.2 Kobe earthquake

3.4 Effective Stress Analysis Using FEM

The workflow followed to carry out the present study is defined precisely in Fig. 5. This study section utilizes the FEM-based non-linear effective stress analysis in OPENSEES. Since the analysis is conducted on the plain strain model, the degree of space (ndm) and degrees of freedom (ndf) are defined as 2 and 3, respectively. The material model used is PM4SAND. The elements assigned are SSPQuadUP, an extension of the SSPquad element for use in dynamic plane strain analysis of fluid-saturated porous media. A mixed displacement-pressure (u-p) formulation is used, based upon the work of Biot as extended by Zienkiewicz and Shiomi (1984). The soil profile is assumed to be almost uniform throughout the 10 m depth, with an upper dense layer located between 1.5 to 2.5 m. The water table is considered at 2 m depth from the ground surface. During the levee construction, densification below the levee is also considered, and permeability is reduced to 100 times in the adjacent soil, 80 times in further below soil layer and so on. The discontinuous permeability in soil layers depicts the soil condition, more close to in-site soil condition (Okamura *et al.* 2001). AFP is evaluated from the excess head profile along the depth which exceeds the hydraulic pressure, *i.e.,* defined as the h_A-line using the formulation given below in Eq. (3).

$$\text{AFP}\ (\text{m}^3) = \int_{z_0}^{z_{GWL}} (h_{\text{exc}} - h_A)^2\, dz \begin{cases} \text{when } h_{exc} > h_A \\ 0, \quad \text{otherwise} \end{cases} \tag{3}$$

where z is the depth from the ground surface; z_{GWL} is the depth of water table from the ground surface; z_o equals 10.0 m, and h_A is the excess head (h_{exc}) required to initiate the artesian flow. At each depth from the ground surface, the h_A value required to cause the artesian flow condition is represented in the soil profile as a line sloping down at 1H:1V from the ground surface. Once AFP is defined, EPI is also estimated by the below Eq. (4):

$$\text{EPI}\ (\text{m}^3 \cdot \text{s}) = \int_{t_o}^{t_f} \int_{z_o}^{z_{GWL}} (h_{\text{exc}} - h_{i_{cr}})^2\, dz\, dt \tag{4}$$

where t_o is the initial time when the input acceleration reaches 0.05g, and $t_f = 150$ s. The t_f of 150 s is assumed based on multiple observations that the typical time of the crust non-liquefiable layer started to crack is approximately 2 to 3 minutes (150 s on average) after the beginning of earthquake shaking from shallow crustal earthquakes (*e.g.,* Ambraseys and Sarma 1969; Bardet and Kapuskar 1993). The ejecta starting time of 2-3 minutes is also consistent with eyewitness accounts during the Canterbury earthquakes.

4. RESULT AND DISCUSSIONS

4.1 Ejecta Manifestation

4.1.1 Model 1 without Levee

Figure 10 shows the visualisation of dynamic behaviour in the form of soil deformation and pore pressure contours for the Model 1 at five time steps (t_1, t_2, t_3, t_4, and t_5) as marked in Fig. 9. Deformed shape as marked in red wireframe is superimposed over black wireframe model structure to trace the relative displacement. As it is evident from the plot, maximum deformations are observed at t_1 and t_2, where applied displacement-time history is maximum in respective positive and negative directions. Initially, a small lateral displacement is observed which increases with time, reaches its peak and then reduces, as discussed in below section. Deformations (15 times magnified) at the end of 40 minutes of shaking are found to be very minimal, with slight lateral drift and negligible settlement. A minimal deformation is expected from level ground soil without levee structure constructed over it, because the entire deformation is under its own self weight, with no overburden of levee.

Contours for excess pore-pressure ratio (R_u) shows that there is no pore-pressure generation up to 2 m depth as the level of the water table is defined at 2 m. R_u is used as an indicator for liquefaction of loose saturated sandy soil under cyclic load tests and is defined by the below Eq. (5).

$$R_u = \frac{\Delta u}{\Delta \sigma'_3} \tag{5}$$

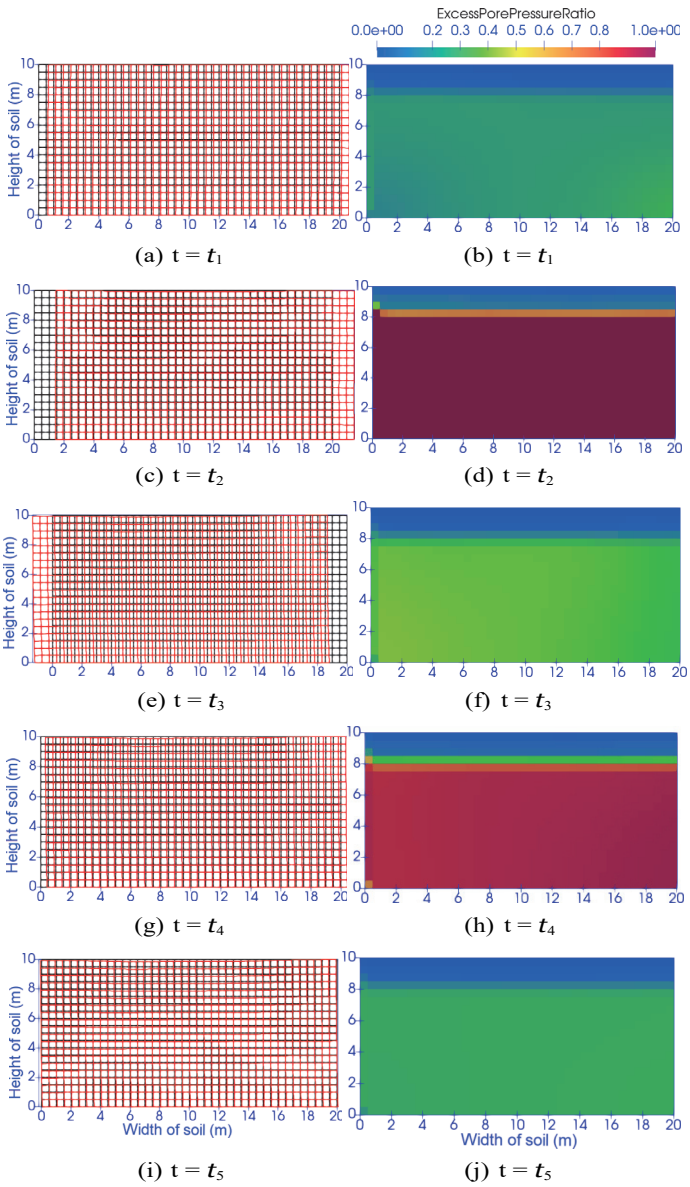

Fig. 10 Output for Model 1. (a), (c), (e), (g), and (i) shows the deformation in soil (magnified to 15 times). (b), (d), (f), (h), and (j) shows the contours for pore pressure generation

where Δu is the excess pore pressure and $\Delta\sigma'_3$ is the effective confining pressure. EPP develops gradually during the initial loading period, but after reaching its maximum value, a sudden drop in EPP is observed. This is the point where liquefaction is initiated. Further application of loading, starts releasing water from pores to the surface, causing the reduction in EPP.

The results for Model 1 are plotted in Fig. 11. The settlement and effective vertical stresses are reported at varying distance along the width of soil column (at x = 3.0, 7.0, 8.5, 11.5, 13.0, and 16.5 m) as shown in Fig. 11(a). The upper soil layers are found to settle more than the subsequent layers as confining pressure increases with the increasing depth from the ground surface, and also because liquefaction is more. Settlement decreases on outer soil layers, as towards the centre of the soil column, the effect of boundary conditions is minimal. An average vertical settlement of magnitude 10 mm is observed in the upper 2 m of the soil. Vertical effective stresses increase linearly along the height of the soil column, reaching a maximum of 110 kPa. There is a small kink at 2 m (Fig. 11(a)). The reason for this kink is that up to 2 m, total stresses and effective stresses are same. But, due to the presence of water table (at 2 m), pore pressure start to has its effect below the water table and reduces the effective stresses.

The hysteresis loops and generation of pore pressures are recorded at a central axis of the soil column (x = 10 m) and plotted for middle and bottom elements as shown in Fig. 11(b). The strain accumulation starts after 10 s of loading, and till the loading continues, shear stresses develops up to ±18 kPa. Similarly, pore-pressure generation occurs up to 10 s and reaches up to 80% in Fig. 11(b), and further it starts dissipating. Pore-pressure ratios reach their maximum of 80% at 10 s and dissipate to 20% till the time loading is applied (40 s). The maximum and dissipated values of pore-pressure ratios decreased with increasing depth from the ground surface since effective confining pressures increase at a higher rate than the excess pore-pressure generation. As per Olson *et al.* (2020), the pore pressure ratio (R_u) between 0.8 to 0.9 is defined as the state of marginal liquefaction and R_u less than 0.8 is defined as the state of no liquefaction. Therefore, it will be true to consider middle layer to liquefy, whereas bottom layer remains non-liquefied. Since the soil at the bottom of the soil Model 1 does not liquefy, the middle liquefiable layer is expected to contribute in sediment ejecta.

Based on the excess head developed, artesian flow potential (AFP) denoting the hydraulic demand is evaluated using Eq. (3). The area of plot of excess head exceeding the h_A-Line represents the hydraulic demand. Variation of hydraulic demand with depth from ground surface is reported at different levels along the width of the soil column, as shown in bar-chart of Fig. 12. The hydraulic demand is maximum at the extreme edges of the model and reduces towards the central axis of the model. The average hydraulic demand considering the section from x = 7 m to x = 13 m, is found to be 7.52 m^3. This demand can produce upto 930 m^3·s of EPI. The evaluations are performed only in the middle section of the model to avoid the boundary effects due to slope topography (Bouckovalas and Papadimitriou 2005; Kishida *et al.* 2009; Tripe *et al.* 2013; Rizzitano *et al.* 2014), which will be affecting the results of Model 2, due to the presence of levee in the considered section. Considering similar section for both models will allow comparing the outcomes for both the models. the This value is huge as compared to the largest sand boils measured in Marina district, Bardet and Kapuskar (1993) (refer Section 1). EPI > 300 m^3·s is categorized as extreme ground failure condition and will have implications on the residential area in the vicinity, which is a matter of concern.

4.1.2 Model 2 with Levee

This section discuss about the effects of sediment ejecta on the levee constructed over liquefiable level ground. Figure 13 shows the visualisation of dynamic behavior in the form of soil deformation and pore pressure contours for the Model 2 at same five time steps (t_1, t_2, t_3, t_4, and t_5) as considered for Model 1. Deformed shape is again marked in red wireframe, that is superimposed over black wireframe model structure to trace the relative displacement. As it is evident from the plot, maximum deformations are observed at t_1 and t_2, where applied displacement-time history is maximum in respective positive and negative directions. Unlike Model 1, Model 2 undergoes lateral displacement as well

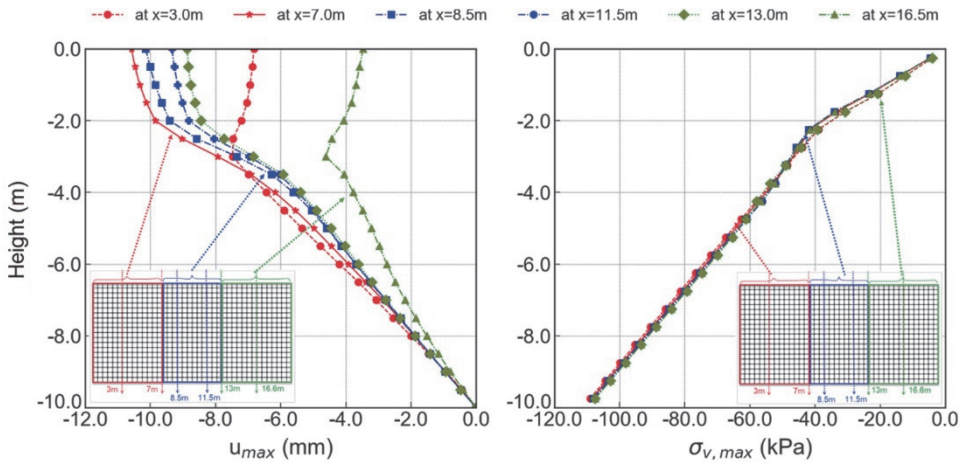

(a) Settlement and effective vertical stress along the depth below ground surface

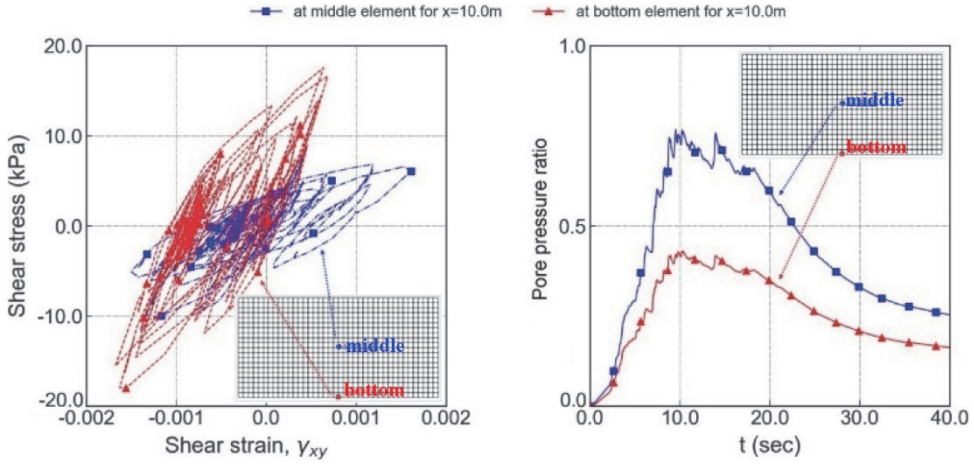

(b) Development of shear stresses and strains and pore-pressure generation with time

Fig. 11 FEA of Model 1 for ejecta evaluation

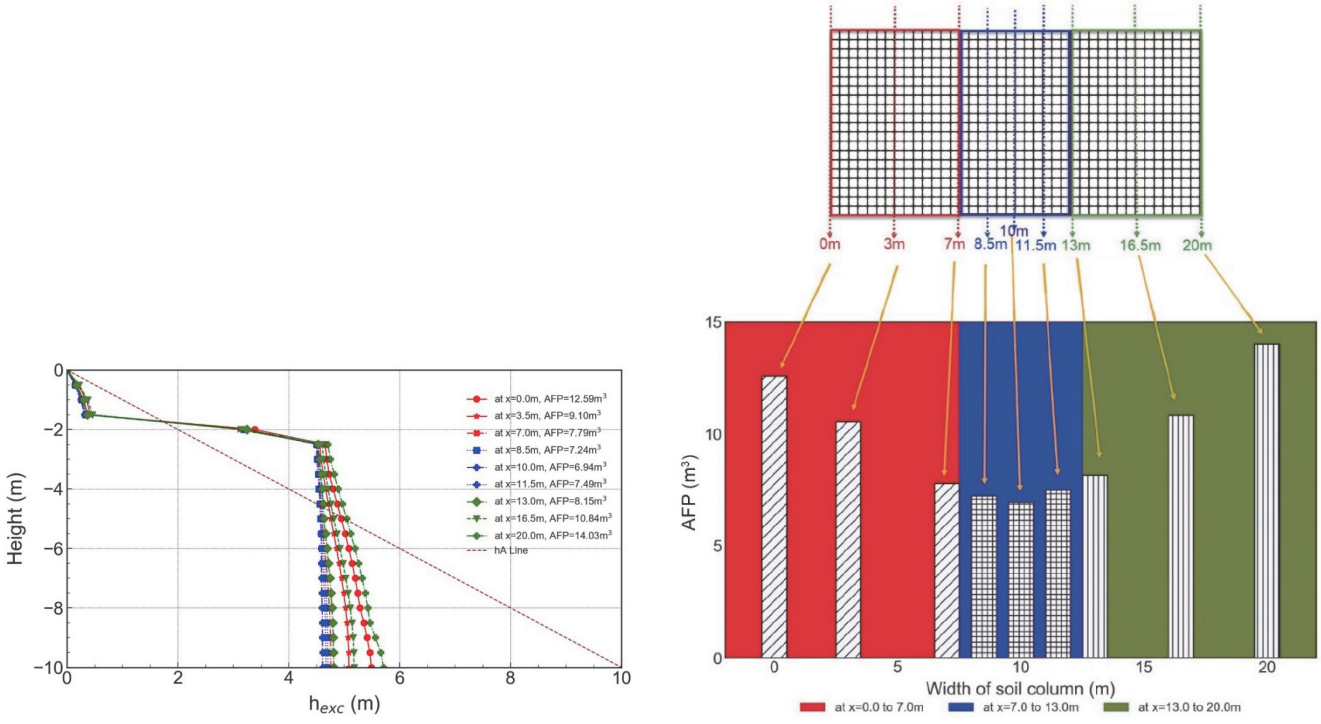

Fig. 12 Hydraulic demand for Model 1, Average AFP = 7.52 m^3

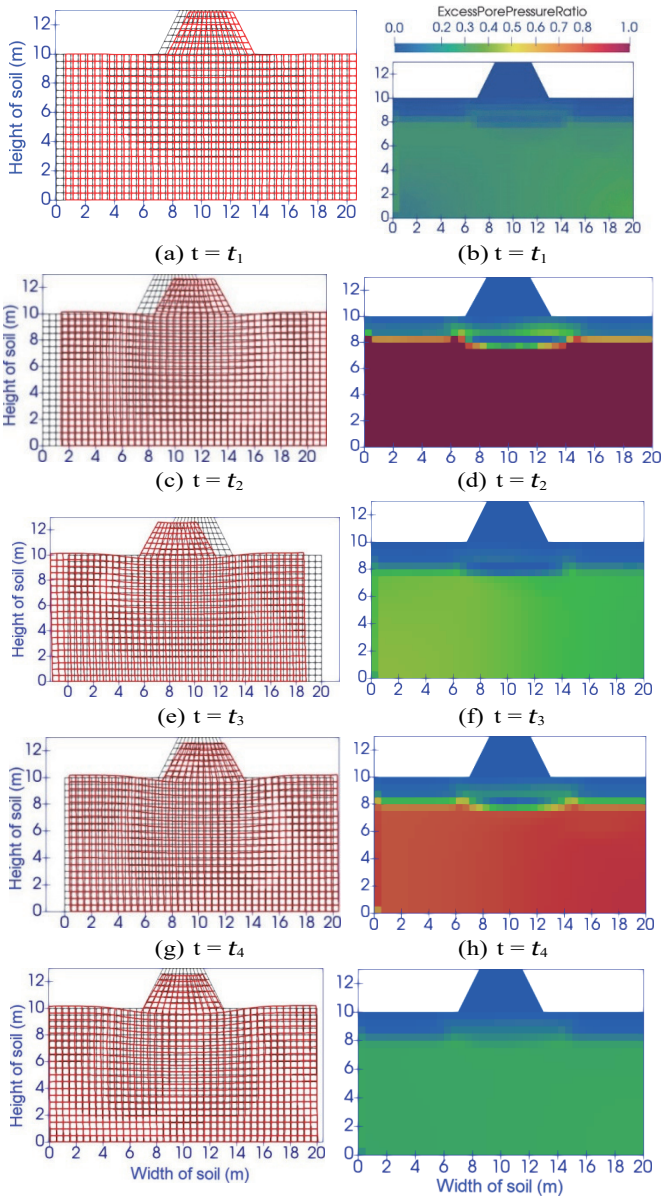

Fig. 13 Output for Model 2. (a), (c), (e), (g), and (i) shows the deformation in soil (magnified to 15 times). (b), (d), (f), (h), and (j) shows the contours for pore pressure generation

as vertical settlement. Initiating with minor deformations, in the later stage of loading magnitude of both lateral displacement and vertical settlement increases with time, reaches its peak and then reduces. The deformations (15 times magnified) at the end of 40 minutes of shaking are found to be larger in comparison to Model 1 (without levee). Levee is observed to punch vertically, that causes upheaving on extreme edges of the soil. Comparatively, larger deformations are expected in Model 2, because additional to the own self weight of soil, there is overburden due to the weight of levee constructed over the soil. Moreover, the developed excess pore pressure remains for a longer period of time at discontinuous low permeability layers compared with the uniform permeability soil deposits (Maharjan and Takahashi (2013); Maharjan and Takahashi (2014)), manifesting a larger settlement.

The contours for excess pore-pressure ratio (EPPR) shows that there is no pore-pressure generation in levee because of the initially assigned completely dry condition to the material used in levee. At the level of water table (2 m), particularly below the levee, a zone of fluctuating excess pore pressures is observed. This is because of the formation of water film beneath the low permeability soil layers below the construction of levee (Kokusho 2000). EPP develops gradually during the initial loading period, but after reaching it's maximum value, suddenly it starts reducing, signifying the occurrence of liquefaction. Further application of loading, starts releasing water from pores to the surface, causing EPP to reduce as was observed in case of Model 1.

The results for Model 2 are plotted in Fig. 14. The settlement and effective vertical stresses are reported at varying distance along the width of soil column (at x = 3.0, 7.0, 8.5, 11.5, 13.0, and 16.5 m) as shown in Fig. 14(a). Similar to Model 1, the upper soil layers are found to deform more than the subsequent layers as confining pressure increases with the increasing height from the ground surface. Also, settlement decreases on outer soil layers, as towards the centre of the soil column, the effect of boundary conditions is minimal. The extreme edges of soil are observed to show positive displacement up to a height of 4 m, because of the upheaving. An average vertical settlement of magnitude 30 mm is observed in the upper 2 m of the soil, which is three times larger than in Model 1. This is due to the high permeability in Model 1 (without levee) compared to Model 2 (with levee), which causes early dissipation of excess pore pressures and lesser time for settlement in Model 1. Vertical effective stresses increase linearly along the height of the soil column, reaching a maximum of 130 kPa. In the case Model 2 also, there is a small kink at 2 m. The reason for this kink is that upto 2 m, total stresses and effective stresses are same. But, due to the presence of water table (at 2 m), pore pressure has it's effect below the water table and reduces the effective stresses.

The hysteresis loops and generation of pore pressures are recorded at a central axis of the soil column (x = 10 m) and plotted for middle and bottom elements as shown in Fig. 14(b). In case of Model 2 also, the strain accumulation starts after 10 s of loading, and till the loading continues, shear stresses develops up to ±21 kPa, which minor increment of 20%. Similarly, positive pore-pressure generation occurs up to 10 s and reaches up to 100%, signifying liquefaction of soil and further it starts dissipating. Pore-pressure ratios reach their maximum of 100% at 10 s and dissipate to 30% till the time loading is applied (40 s). The increments in maximum and dissipated values in Model 2 than it was found in Model 1 are 25% and 50% respectively. The maximum and dissipated values of pore-pressure ratios decreased with increasing depth from the ground surface since effective confining pressures increase at a higher rate than the excess pore-pressure generation. In Model 2 also, the middle liquefiable soil contributes to sediment ejecta, whereas the soil at the bottom of the soil seems to remain in a state of no liquefaction.

Based on the excess head developed, artesian flow potential (AFP) denoting the hydraulic demand is evaluated using Eq. (3). The method of estimation remains similar to that used for Model 1. The area of plot of excess head exceeding the h_A-Line represents the hydraulic demand. Variation of hydraulic demand with depth from ground surface is reported at different levels along the width of the soil column, as shown in bar-chart of Fig. 15. The hydraulic demand is maximum at the extreme edges of the model and reduces towards the central axis of model. The average hydraulic demand of sediment ejecta considering the middle section of the model 2, *i.e.,* below the levee, is found to be 5.49 m^3. This demand

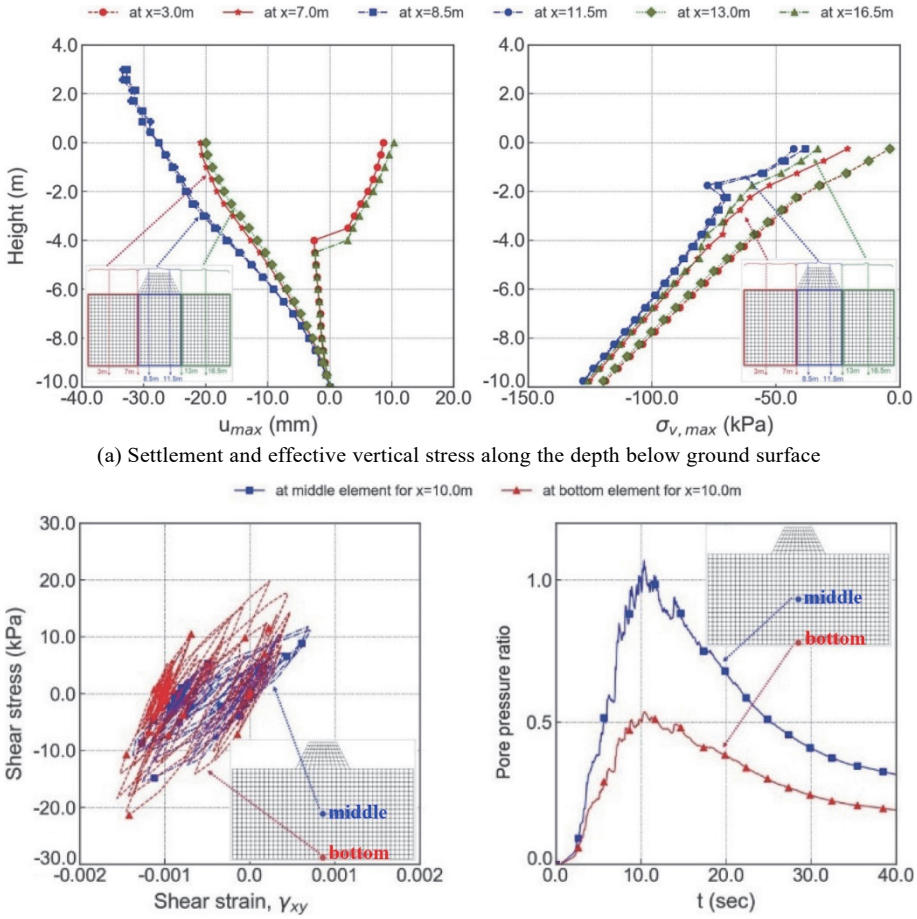

(a) Settlement and effective vertical stress along the depth below ground surface

(b) Development of shear stresses and strains and pore-pressure generation with time

Fig. 14 FEA of Model 2 with levee constructed over it for ejecta evaluation

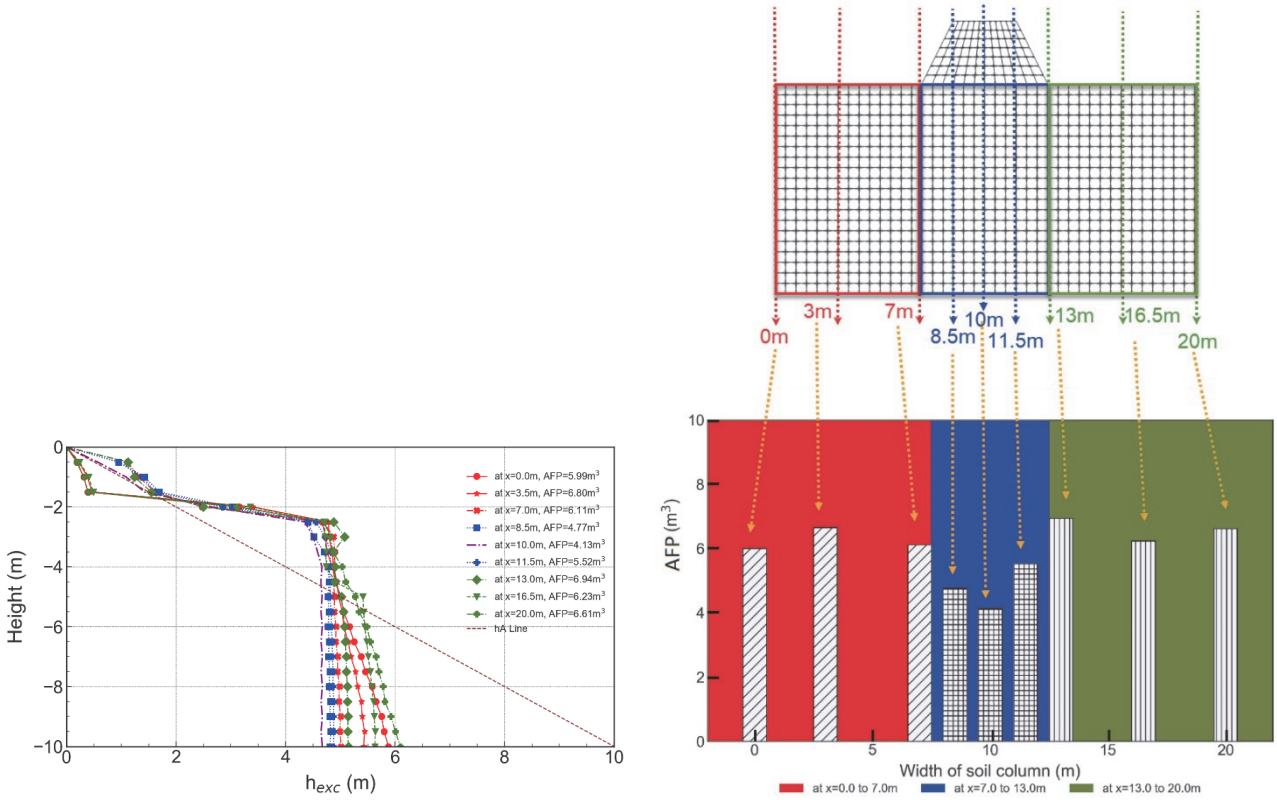

Fig. 15 Hydraulic demand for Model 2, Average AFP = 5.49 m³

can produce upto 680 $m^3 \cdot s$ of EPI, which is less than that estimated in model 1, but individually it is also significant and expected to create extreme ground failure condition. This is a matter of concern, because it has caused accumulation of excess pore pressures beneath the levee, which will further lead to ground subsidence and will make the levee unstable. Also, since EPP is not finding vertical path to escape, flow takes place from the edges of levee, creating discontinuity along that path and making soil weaker in strength.

4.2 Flow Analysis

Figure 16 shows the direction of flow of pore water, which is seen to be vertically upwards (Figs. 16(a), 16(c), 16(e), and 16(g)) in the case of the Model 1, but goes outward (Figs. 16(b), 16(d), 16(f), and 16(h)) in the Model 2 having constructed levee. Due to the construction of the levee, permeability is decreased below the levee, causing water to flow towards the locations with higher permeability. This deviation is also dependent on the magnitude of loading, because of this, outward flow of sediments is more upto 25 s of loading, and reduces beyond. Due to the construction of levee, the permeability is reduced by 100 times just below the construction, and this reduces with depth of soil. This is reflected in flow path

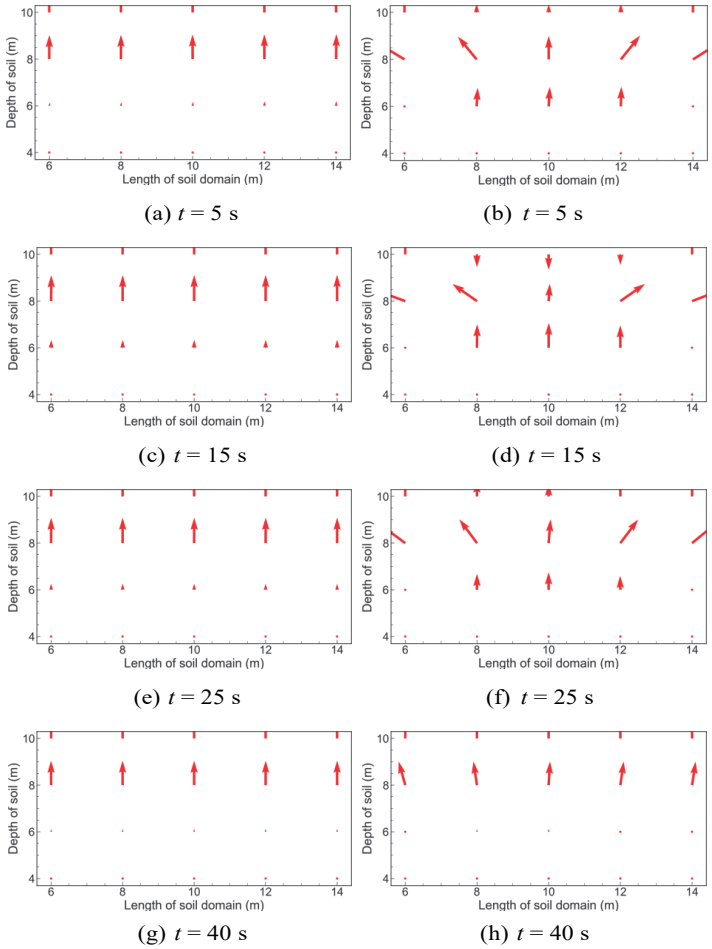

Fig. 16 The flownet for Model 1 (without levee) is presented in (a), (c), (e), and (g) and the flownet for Model 2 (with levee) is presented in (b), (d), (f), and (h)

of pore fluid, as there is no deviation observed below 6 m. The ground below the construction of levee has become non-homogenous due to difference in permeability which reduces further with depth from ground surface. This non-uniformity could be due to void-ratio re-distribution, where voids re-arrange themself in search of a stable position. The sediment ejecta flows out of the ground surface due to the cavities formed within the soil, which in the present explanation are referred to as discontinuity in soil, caused due to void ratio redistribution. Thus, knowing the path of flow of sediment ejecta, the possible places for ground improvement can be identified, which can reduce these cavities. This will help to increase the strength of soil and further reduce the sediment ejecta. However, introducing discontinuity is not a part of the present study but is considered for the future scope of the work.

5. SUMMARY

In the presented work, sediment ejecta manifestation is studied. The effect of sediment ejecta on the dynamic behaviour of a levee constructed over liquefiable soil is examined using an effective stress analysis using the finite element approach. Initially, it is essential to know the behaviour of level liquefiable ground during an earthquake. Therefore, two models are analysed simultaneously: Model 1 (without levee) and model 2 (with levee). Sediment ejecta is manifested for both the models, followed by studying fluid flow path for individual cases. The major findings are as follows:

1. The hydraulic demand and ground failure severity are measured in Models 1 (no levee) and 2 (with levee). The hydraulic demand by the levee is 5.49 m^3 producing 680 $m^3 \cdot s$ EPI, which is substantial to cause sediment ejecta on a large scale and might harm the built environment causing extreme ground failure conditions.
2. In the upper 2 m of the soil, an average settlement of 10 and 30 mm are observed in Model 1 (without levee) and Model 2 (with levee), respectively. The more significant deformations are expected in Model 2 because due to the formation of a thin film of water, the development of excess pore pressures remains for a more extended period due to low permeability. It allows the soil to lose strength and causes more significant ground subsidence.
3. The flow path of pore fluid indicates a diversion of pore-water flow towards the region of high permeability in Model 2 (with levee). In contrast, the flow is vertical in Model 1 (without a levee). The diversion could be the non-homogeneity in the ground due to differential permeability which reduces further with depth from the ground surface. This non-uniformity could be due to void-ratio re-distribution, where the re-arrangement of voids occurs to achieve stabilization.
4. Effect of sediment ejecta on the levee constructed over liquefiable ground is significant as it introduces discontinuity within the model ground and affects the dynamic stability of the levee.
5. Evaluation of hydraulic demand and qualitatively estimating the sediment ejecta produces a reliable estimate for adopting cost-effective and efficient measurements to increase the stiffness of soil, which can be studied separately and considered for future scope of the work.

6. Results have shown that the slope topography affects the results due to boundary effects, which itself opens a wide scope for future recommendations. The effect of model dimensions and slope topography can be further studied on ejecta manifestation.

ACKNOWLEDGEMENT

The authors thank the Department of Earthquake Engineering for providing the well-equipped resources required for experimental and numerical studies. Special mention to Mr. Digvijay Patankar, a research scholar at IIT Roorkee, for his contribution in resolving coding bugs.

FUNDING

The authors have received funds from Faculty Initiation Grant, FIG100915, for newly joined faculty members. The authors also thank the Ministry of Human Resource Development, MHRD, for scholarships to Indian scholars under their research scheme.

DATA AVAILABILITY

Most of it is provided in the manuscript, and the remaining is available upon request.

CONFLICTS OF INTEREST

The authors have no conflicts of interest to declare relevant to this article's content. Any opinions, findings, conclusions or recommendations expressed in this material are those of the authors and do not necessarily reflect the views of the funding agencies.

REFERENCES

Ambraseys, N. and Sarma, S. (1969). "Liquefaction of soils induced by earthquakes." *Bulletin of the Seismological Society of America*, **59**(2), 651-664. https://doi.org/10.1785/bssa0590020651

Ashford, S., Boulanger, R., Donahue, J., and Stewart, J. (2011). *Geotechnical Quick Report on the Kanto Plain Region during the Japan.* GEER Report-025a. https://doi.org/10.18118/G64S3W

Bardet, J. and Kapuskar, M. (1993). "Liquefaction sand boils in San Francisco during 1989 Loma Prieta earthquake." *Journal of Geotechnical Engineering*, **119**(3), 543-562. https://doi.org/10.1061/(ASCE)0733-9410(1993)119:3(543)

Been, K. and Jefferies, M. (1985). "A state parameter for sands." *Géotechnique*, **35**(2), 99-112. https://doi.org/10.1680/geot.1985.35.2.99

Biot, M. (1956). "Theory of propagation of elastic waves in a fluid-saturated porous solid. i. low-frequency range." *The Journal of the Acoustical Society of America*, **28**(2), 168-178. https://doi.org/10.1121/1.1908239

Biot, M. (1962a). "Mechanics of deformation and acoustic propagation in porous media." *Journal of Applied Physics*, **33**(4), 1482-1498. https://doi.org/10.1063/1.1728759

Biot, M. (1962b). "Generalized theory of acoustic propagation in porous dissipative media." *The Journal of the Acoustical Society of America*, **34**(9A), 1254-1264. https://doi.org/10.1121/1.1918315

Biot, M. (1941). "General theory of three-dimensional consolidation." *Journal of Applied Physics*, **12**(2), 155-164. https://doi.org/10.1063/1.1712886

Bolton, M.D. (1986). "The strength and dilatancy of sands." *Géotechnique*, **36**(1), 65-78. https://doi.org/10.1680/geot.1986.36.1.65

Bouckovalas, G.D. and Papadimitriou, A.G. (2005). "Numerical evaluation of slope topography effects on seismic ground motion." *Soil Dynamics and Earthquake Engineering*, **25**(7-10), 547-558. https://doi.org/10.1016/j.soildyn.2004.11.008

Boulanger, R. and Ziotopoulou, K. (2015). *PM4SAND (Version 3): A Sand Plasticity Model for Earthquake Engineering Applications*. https://doi.org/Reportno.UCD/CGM-12/01,centerforGeotechnicalModeling

Chen, L. and Arduino, P. (2020). *Implementation, Verification, and Validation of the PM4SAND Model in Opensees*, Tech. Rep. Seattle, WA, Pacific Earthquake Engineering Research Center, University of California, Berkeley, CA. https://doi.org/10.55461/sjeu6160

Cubrinovski, M., Rhodes, A., Ntritsos, N., and Van Ballegooy, S. (2019). "System response of liquefiable deposits." *Soil Dynamics and Earthquake Engineering*, **124**, 212-229. https://doi.org/10.1016/j.soildyn.2018.05.013

Dafalias, Y.F. and Manzari, M.T. (2004). "Simple plasticity sand model accounting for fabric change effects." *Journal of Engineering Mechanics*, ASCE, **130**(6), 622-634. https://doi.org/10.1061/(ASCE)0733-9399(2004)130:6(622)

Harder, L., Kelson, K.I., and Kishida, T. (2011). *Preliminary Observations of Levee Performance and Damage Following the March 11, 2011 Tohoku Offshore Earthquake, Japan.* https://doi.org/Reportnumber:GEERAssociationReportNo.GEER-025B

Housner, G. (1958). "The mechanism of sandblows." *Bulletin of the Seismological So-ciety of America*, **48**(2), 155-161. https://doi.org/10.1785/bssa0480020155

Hutabarat, D. and Bray, J. (2019). "Effective stress analysis of liquefiable site in christchurch to discern the characteristics of sediment ejecta." *Earthquake Geotechnical Engineering for Protection and Development of Environment and Constructions*, 2923-2931. CRC Press. https://www.issmge.org/publications/online-library

Hutabarat, D. and Bray, J. (2021). "Effective stress analysis of liquefiable sites to estimate the severity of sediment ejecta." *Journal of Geotechnical and Geoen-Vironmental Engineering*, ASCE, **147**(5), 04021024. https://doi.org/10.1061/(asce)gt.1943-5606.0002503

IS1893:Part1. (2016). *Criteria for Earthquake Resistant Design of Strucrures: General Provisions and Buildings*. Bureau of Indian Standards, New Delhi, India.

Kawai, T., Kim, J., Kazama, M., and Yoshii, T. (2017). "An experimental study of sand boiling in relation to shearing characteristics of liquefied soil". *19th International Conference on Soil Mechanics and Geotechnical Engineering, ICSMGE*. https://www.issmge.org/publications/online-library

Kirar, B. and Maheshwari, B. (2018). "Dynamic properties of soils at large strains in roorkee region using field and laboratory tests." *Indian Geotechnical Journal*, **48**(1), 125-141. https://doi.org/10.1007/s40098-017-0258-2

Kishida, T., Boulanger, R.W., Abrahamson, N.A., Driller, M.W., and Wehling, T.M. (2009). "Seismic response of levees in the sacramento-san joaquin delta." *Earthquake Spectra*, **25**(3), 557-582. https://doi.org/10.1193/1.3157259

Kokusho, T. (2000). "Mechanism for water film generation and lateral flow in liquefied sand layer." *Soils and Foundations*, **40**(5), 99-111. https://doi.org/10.3208/sandf.40.5_99

Lowe, D. (1975). "Water escape structures in coarse-grained sediments." *Deep-Water Turbidite Systems*, **22**, 114-114. Blackwell Publishing Ltd. https://doi.org/10.1002/9781444304473.ch10

Maharjan, M. and Takahashi, A. (2013). "Effects of nonhomogeneity on liquefaction in stratified soil deposits." *10th International Conference for Urban Earthquake Engineering*, 483-492.

Maharjan, M. and Takahashi, A. (2014). "Liquefaction-induced deformation of earthen embankments on non-homogeneous soil deposits under sequential ground motions." *Soil Dynamics and Earthquake Engineering*, **66**, 113-124. https://doi.org/10.1016/j.soildyn.2014.06.024

Manzari, M.T. and Dafalias, Y.F. (1997). "A critical state two-surface plasticity model for sands." *Géotechnique*, **47**(2), 255-272. https://doi.org/10.1680/geot.1997.47.2.255

Matsuo, O. (1996). "Damage to River Dikes." *Soils and Foundations, Special Issue on Geotechnical Aspects of the January 17, 1995 Hyogoken-Nambu Earthquake*, 235-240. https://doi.org/10.3208/sandf.36.Special 235

Maurer, B., Green, R., Cubrinovski, M., and Bradley, B. (2014). "Evaluation of the liquefaction potential index for assessing liquefaction." *Journal of Geotechnical and Geoenvironmental Engineering*, ASCE, **140**(7). https://doi.org/10.1061/(ASCE)GT.1943-5606.0001117

NAS. (1985). *Liquefaction of Soils during Earthquakes*. National Academies of Sciences, Engineering, and Medicine, Washington, DC. https://doi.org/10.17226/19275

NAS. (2016). *State of the Art and Practice in the Assessment of Earthquake-Induced Soil Liquefaction and Its Consequences*. National Academies of Sciences, Engineering, and Medicine, Washington, DC. https://doi.org/10.17226/23474

Oka, F., Tsai, P., Kimoto, S., and Kato, R. (2012). "Damage patterns of river embankments due to the 2011 off the pacific coast of tohoku earthquake and a numerical modeling of the deformation of river embankments with a clayey subsoil layer." *Soils and Foundations*, **52**(5), 890-909. https://doi.org/10.1016/j.sandf.2012.11.010

Okamura, M., Abdoun, T.H., Dobry, R., Sharp, M.K., and Taboada, V.M. (2001). "Effects of sand permeability and weak aftershocks on earthquake-induced lateral spreading." *Soils and Foundations*, **41**(6), 63-77. https://doi.org/10.3208/sandf.41.6 63

Olson, S.M., Mei, X., and Hashash, Y.M. (2020). "Nonlinear site response analysis with pore-water pressure generation for liquefaction triggering evaluation." *Journal of Geotechnical and Geoenvironmental Engineering*, ASCE, **146**(2), 04019128. https://doi.org/https://doi.org/10.1061/(ASCE)GT.1943-5606.0002191

Rizzitano, S., Cascone, E., and Biondi, G. (2014). "Coupling of topographic and stratigraphic effects on seismic response of slopes through 2d linear and equivalent linear analyses." *Soil Dynamics and Earthquake Engineering*, **67**, 66-84. https://doi.org/10.1016/j.soildyn.2014.09.003

Sasaki, Y., Towhata, I., Miyamoto, K., Shirato, M., Narita, A., Sasaki, T., and Sako, S. (2012). "Reconnaissance report on damage in and around river levees caused by the 2011 off the pacific coast of tohoku earthquake." *Soils and Foundations*, **52**(5), 1016-1032. https://doi.org/https://doi.org/10.1016/j.sandf.2012.11.018

Seed, H. (1979). "Soil liquefaction and cyclic mobility evaluation for level ground during earthquakes." *Journal of the Geotechnical Engineering Division*, **105**(2), 201-255. https://doi.org/10.1061/ajgeb6.0000768

Selig, E. and Ladd, R. (1978). "Preparing test specimens using undercompaction." *Geotechnical Testing Journal*, **1**(1), 16. https://doi.org/10.1520/gtj10364j

Soga, K. (1998). "Soil liquefaction effects observed in the kobe earthquake of 1995." *Proceedings of the Institution of Civil Engineers—Geotechnical Engineering*, **131**(1), 34-51. https://doi.org/10.1680/igeng.1998.30004

Takada, N., Nishi, M., and Fukuda, M. (1996). "Damage to river levees and revet-ments." *Soils and Foundations*, **36**, 241-254. https://doi.org/10.3208/sandf.36.Special 241

Takano, D., Morikawa, Y., and Takahashi, H. (2016). "Centrifuge modeling of sand boil on sand containing silt." *Japanese Geotechnical Society Special Publication*, **2**(23), 875-879. https://doi.org/https://doi.org/10.3208/jgssp.JPN-139

Tobita, T. (2019). "Mechanism of liquefaction-induced settlements with sand boiling." *The 16th Asian Regional Conference on Soil Mechanics and Geotechnical Engineering*.

Towhata, I. (2014). "Geotechnical earthquake engineering: Damage mechanism observed." M. Beer, I. A. Kougioumtzoglou, E. Patelli, & I. S.-K. Au (Eds.), *Encyclopedia of Earthquake Engineering*, 1-29. Springer Berlin Heidelberg. https://doi.org/10.1007/978-3-642-36197-5_2-1

Tripe, R., Kontoe, S., and Wong, T. (2013). "Slope topography effects on ground motion in the presence of deep soil layers." *Soil Dynamics and Earthquake Engineering*, **50**, 72-84. https://doi.org/https://doi.org/10.1016/j.soildyn.2013.02.011

Tsai, C.-C., Lin, W.-C., Chu, M.-C., and Chi, C.-C. (2022). "Experimental study on the mechanism of sand boils and associated settlements due to soil liquefaction in loose sand." *Engineering Geology*, **306**, 106708. https://doi.org/10.1016/j.enggeo.2022.106708

van Ballegooy, S., Wentz, F., and Boulanger, R. (2015). "Evaluation of cpt-based liquefaction procedures at regional scale." *Soil Dynamics and Earthquake Engineering*, **79**, 315-334. https://doi.org/10.1016/j.soildyn.2015.09.016

Zienkiewicz, O. and Shiomi, T. (1984). "Dynamic behaviour of saturated porous media; the generalized biot formulation and its numerical solution." *International Journal for Numerical and Analytical Methods in Geomechanics*, **8**(1), 71-96. https://doi.org/10.1002/nag.1610080106